Supplemental Figure 1. Filipescu et al.

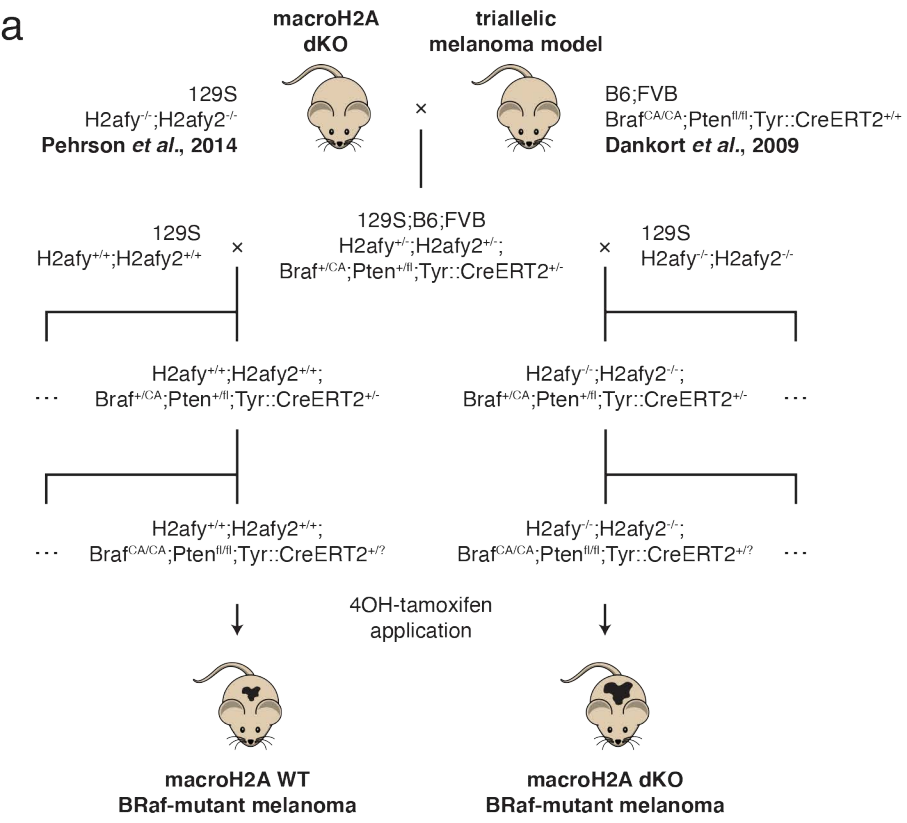

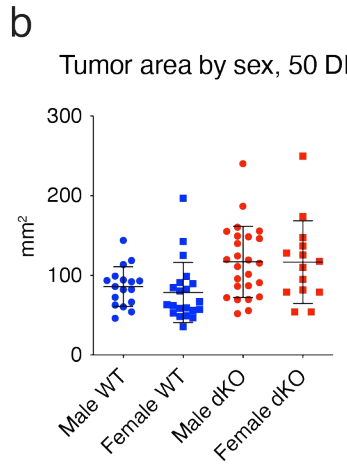

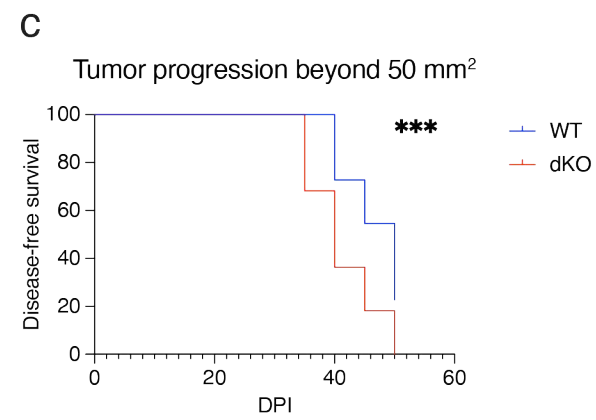

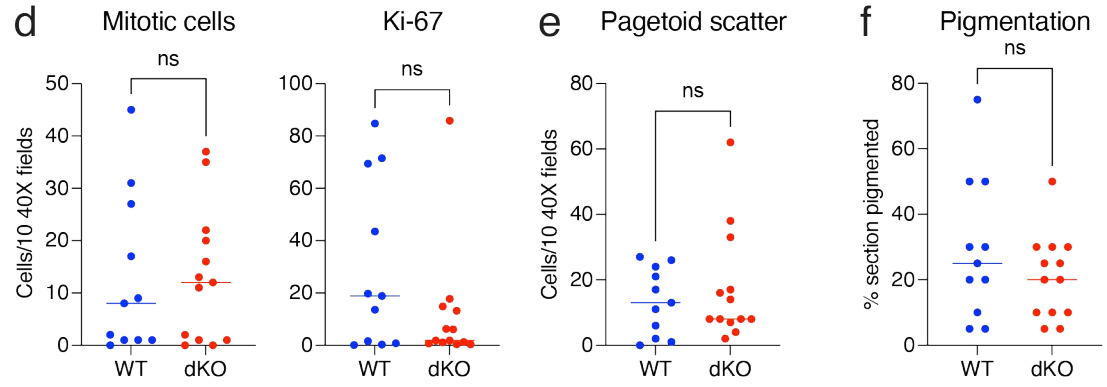

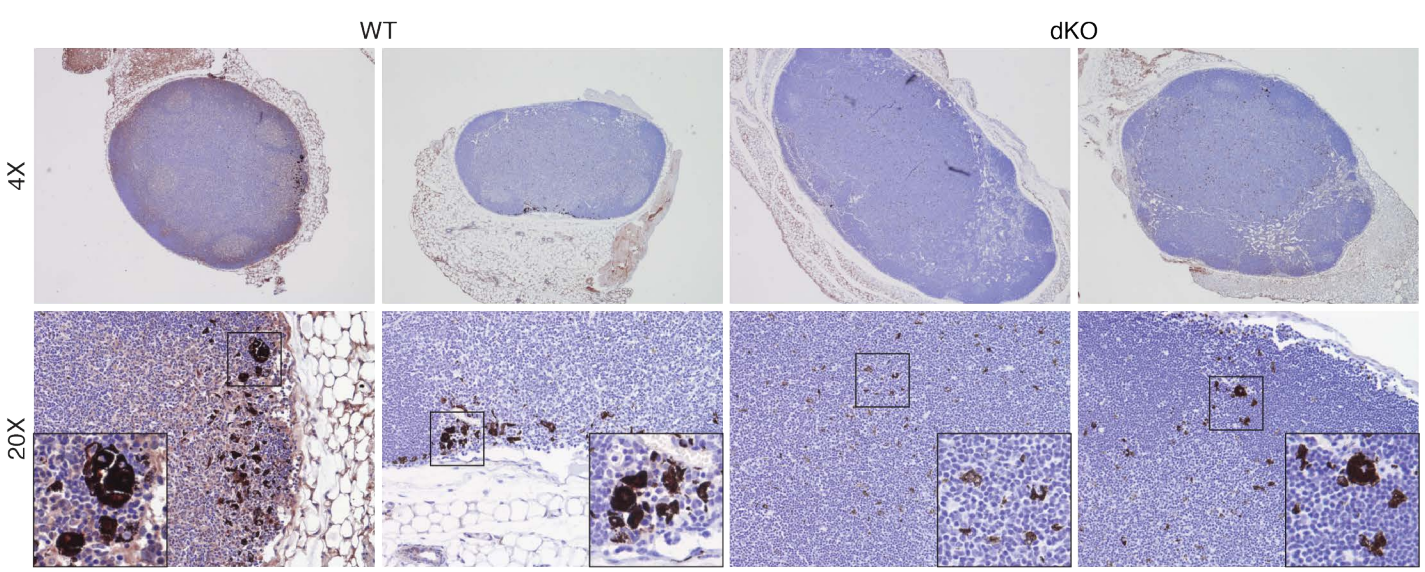

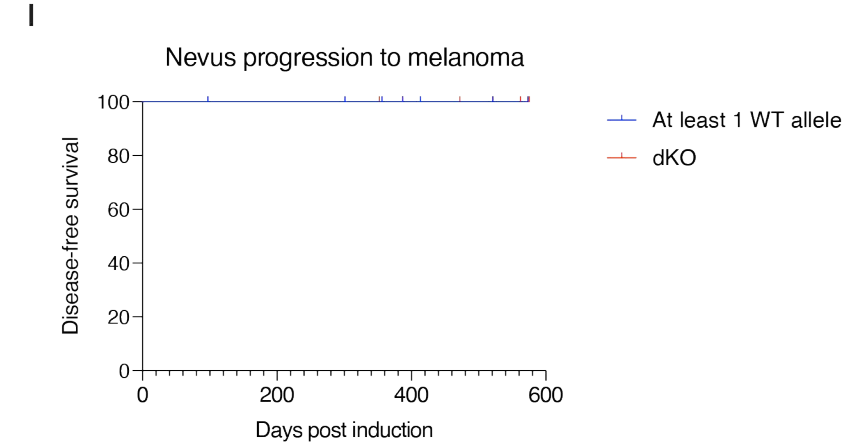

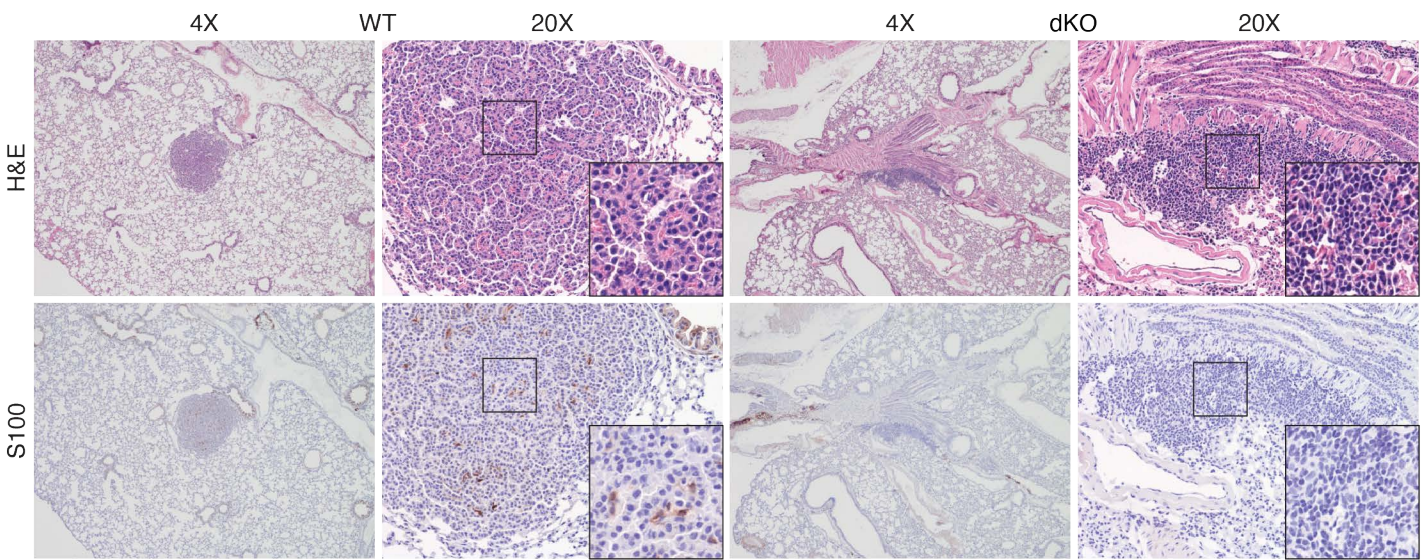

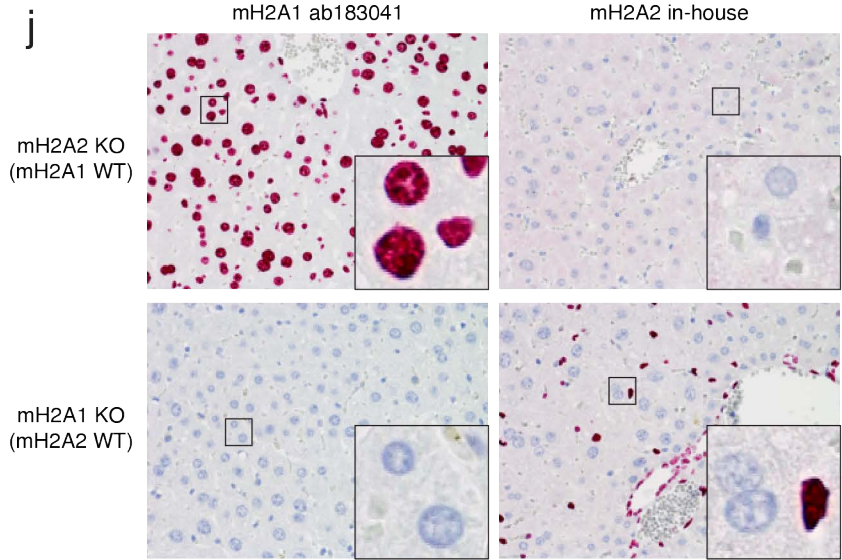

Supplemental Figure 1. Characterization of macroH2A WT and dKO murine melanomas

a) Breeding strategy used to produce mice used for melanoma induction in the presence and absence of macroH2A. b) Tumor area in males and females of indicated genotypes. No significant inter-sex differences were observed (Kruskal-Wallis test corrected for multiple comparisons). c) Kaplan-Meier analysis of disease-free survival following melanoma induction. Events correspond to melanoma growth beyond an area of 50 mm^2. P-value = 0.0009, log-rank (Mantel-Cox) test. d) Proliferation analysis at 50 DPI by immunohistochemical detection of the mitotic marker H3S10ph and Ki-67. Ten random fields were scored per tumor. e) Analysis of pagetoid spread of melanocytic cells into epidermal structures. Ten epidermis-containing fields were scored per tumor on H&E-stained sections. f) Relative area of the tumor containing pigmented cells, estimated on a 2X magnification ensemble view of H&E-stained sections. d-f, significance determined using a Mann-Whitney test. g) Sections of tumor-draining axillary lymph nodes stained for S100 (reddish-brown NovaRed substrate color), showing isolated pigmented cells but lack of S100-positive overt metastases. 4X and 20X magnification shown; inserts shown at 2.5X additional magnification. h) Lung sections of tumor-bearing mice at 50 DPI. Detected lesions lack S100 staining or typical melanoma morphology. 4X and 20X magnification shown; inserts shown at 2.5X additional magnification. i) Kaplan-Meier analysis of disease-free survival following nevus induction. Progression to melanoma was defined as radial and/or vertical lesion growth but was not observed during the lifespan of the mice. j) Validation of antibody specificity in immunohistochemistry, using liver of either macroH2A1 or macroH2A2 single KO mice. 20X magnification, inserts shown at 5X additional magnification.

Supplemental Figure 2. Filipescu et al.

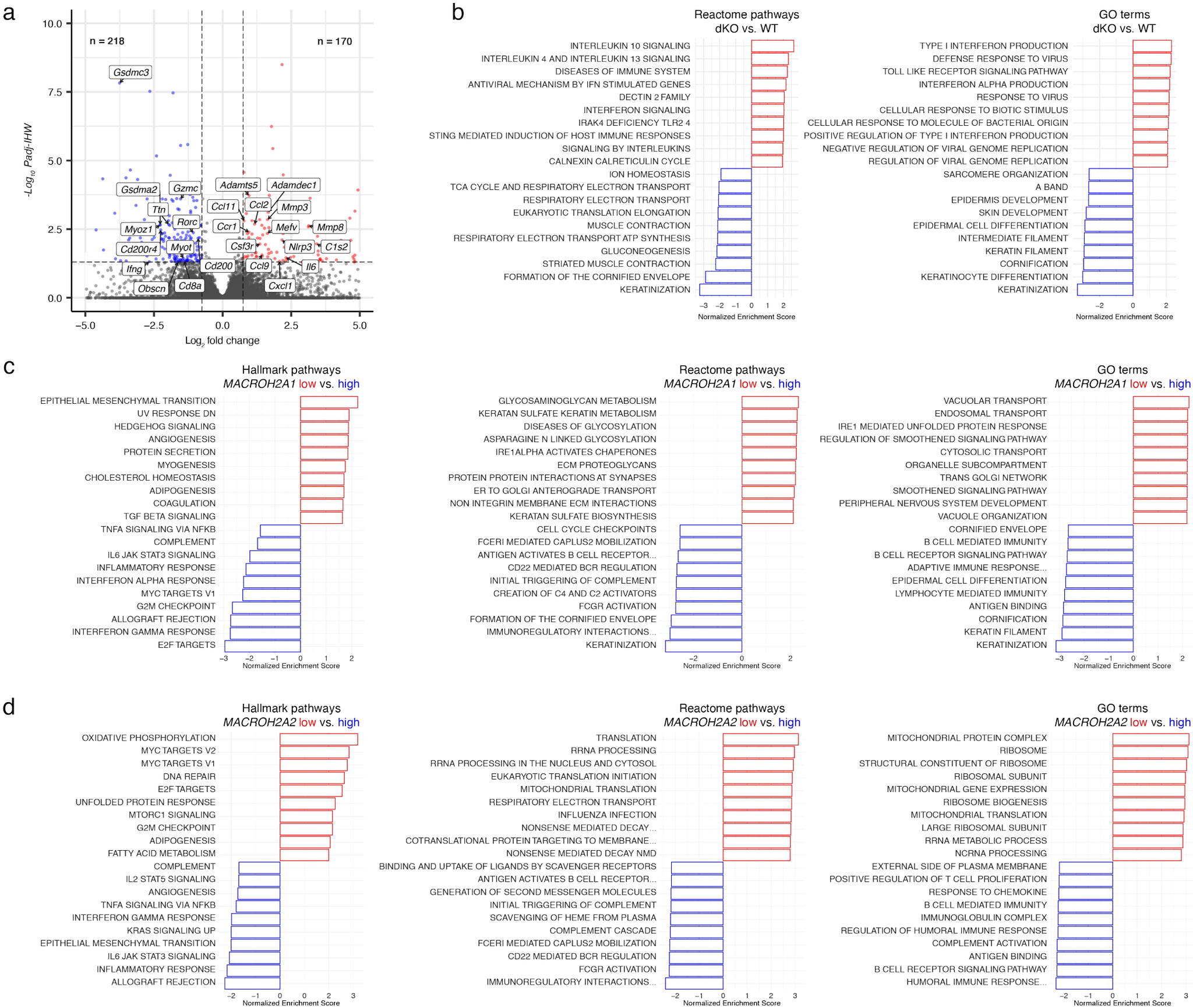

Supplemental Figure 2. Murine macroH2A-deficient and human macroH2A^{low} melanomas deregulate gene pathways associated with immune anti-tumor response

a) Volcano plot of differential gene expression in dKO vs. WT murine melanomas analyzed by RNA-seq. Significantly DEGs are colored: red = up in dKO and blue = down in dKO. X and Y axes are zoomed in to show genes of interest. Genes in Figure 2b are depicted. b) GSEA analysis of Reactome pathways and GO terms in dKO vs. WT murine melanomas. Top 10 significant pathways shown. c, d) Top 10 significant Hallmark, Reactome pathways and GO terms in GSEA analysis of *MACROH2A1* and *MACROH2A2* low vs. high metastatic melanomas from the TCGA cohort, respectively.

Supplemental Figure 3. Filipescu et al.

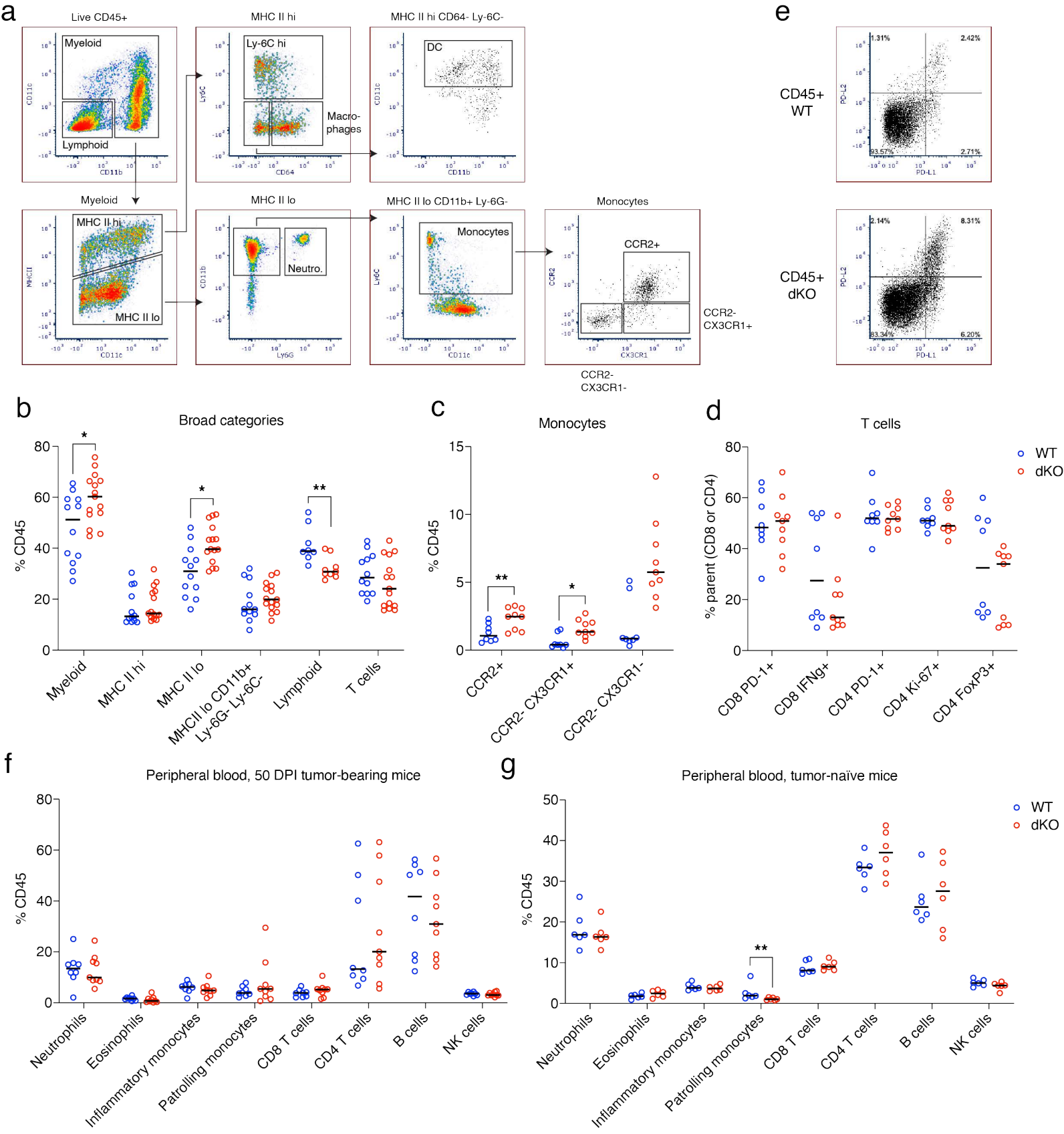

Supplemental Figure 3. Flow cytometric analysis of macroH2A WT and dKO melanoma-infiltrating and circulating immune cell populations

A: Gating strategy used to delineate tumor-infiltrating myeloid cell subtypes by flow cytometry, shown in a WT tumor. b) Broad immune cell categories not shown in Figure 3 at 50 DPI. c) Relative abundance of monocyte subpopulations identified by CCR2 and CX3CR1 expression. d) Analysis of additional markers of T cell functionality. e) PD-L1 and PD-L2 staining of CD45+ cells infiltrating WT and dKO melanomas. f, g) Quantification of indicated populations of non-overlapping peripheral blood immune cell populations at 50 DPI, and in tumor-naïve mice, respectively, determined by flow cytometry. Mann-Whitney test P-values shown for all panels: * < 0.05, ** < 0.01.

Supplemental Figure 4. Filipescu et al.

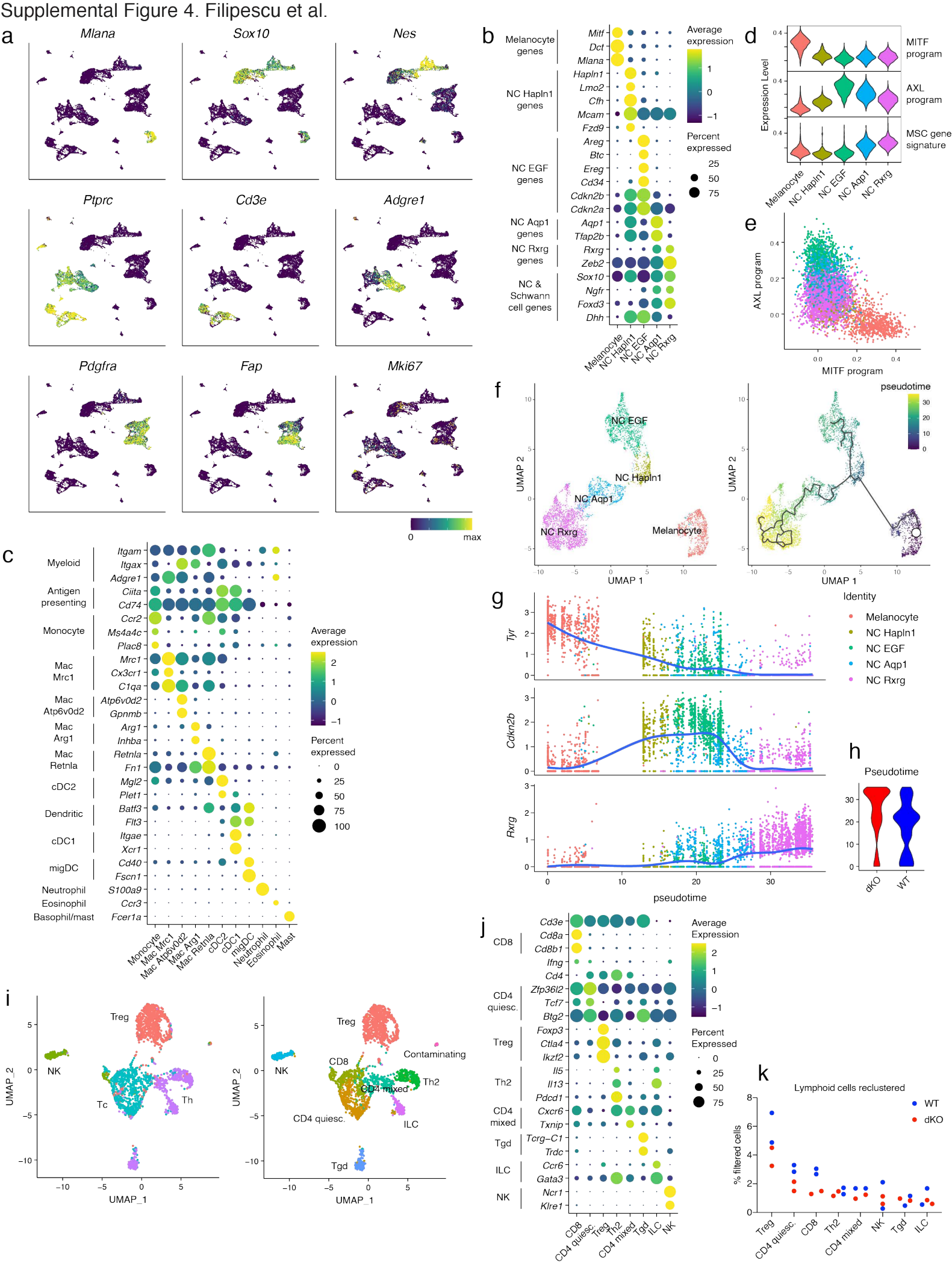

Supplemental Figure 4. Details of scRNA-seq analysis to annotate components of the melanoma TME

a) Expression of marker genes used to delineate major cell lineages expected in the TME, shown on UMAP plots. b, c) Selected cluster-specific markers used to annotate cell types/states of the neural crest (NC) lineage and myeloid lineage, respectively. d) Violin plots of indicated gene expression signatures measured across NC clusters. e) Scatter plot of antagonistic MITF and AXL-driven gene expression signatures identified in human melanoma, across NC clusters in (d). f) Pseudotime analysis of reclustered NC cells performed with Monocle. Left, original neural crest clusters after re-integration, dimensionality reduction and UMAP embedding. Right, cell trajectories in pseudotime anchored in the melanocyte cluster (white circle). g) Representation of expression profiles of key genes across pseudotime in NC clusters. h) Violin plots of pseudotime values across dKO and WT NC cells. i) UMAP plot of lymphoid cells after re-integration, dimensionality reduction and UMAP embedding, labeled according to their original clusters (left) and annotations generated by reclustering (right). j) Selected markers used to annotate lymphoid cell types/states following reclustering in (i). k) Relative frequencies across lymphoid clusters as annotated in (i) and (j).

Supplemental Figure 5. Filipescu et al.

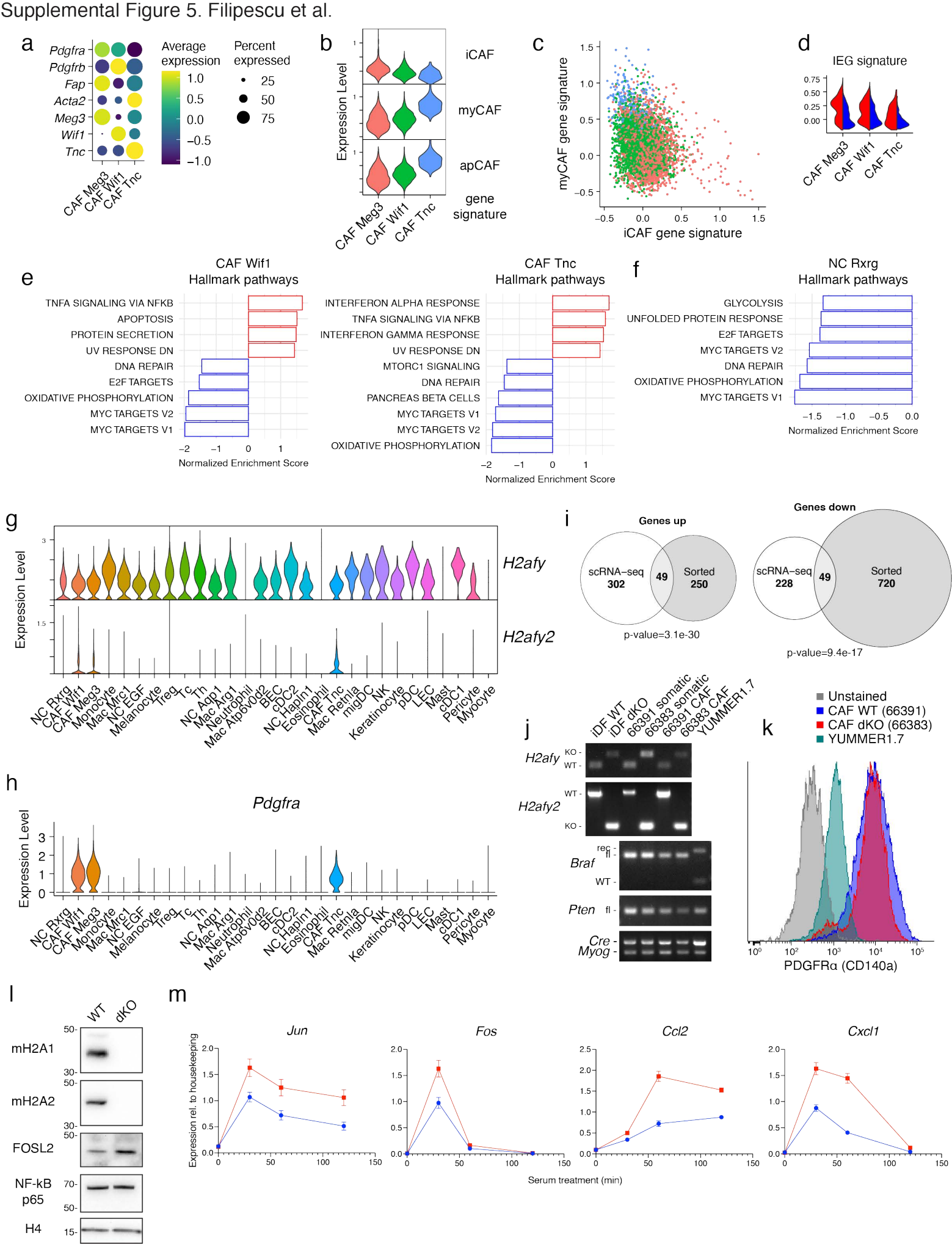

Supplemental Figure 5. Characterization of CAF clusters in the melanoma TME and their *in vitro* counterparts

a) Dot plot of selected markers used to annotate CAFs, and CAF cluster specific genes *Meg3*, *Wif1* and *Tnc*. b) Violin plots of gene expression signatures characterizing murine pancreatic cancer CAF populations measured across murine melanoma CAF clusters. c) Scatter plot of inflammatory and myocyte-like CAF gene expression signatures identified in pancreatic cancers showing a lack of distinction among murine melanoma CAF clusters. d) Violin plot of an immediate early gene (IEG) signature in CAFs. Significant dKO vs. WT differences are present within each cluster (Wilcoxon rank sum test adjusted P-value < 0.05, cluster-average log2 fold change > 0.1). e, f) Significant Hallmark pathways in GSEA analysis of dKO vs. WT performed in CAF Wif1 and CAF Tnc clusters, and NC Rxrg cluster, respectively g) Violin plots showing macroH2A gene expression across cell types/states in the melanoma TME. h) Violin plot of *Pdgfra* gene expression across cell types/states in the melanoma TME demonstrates its specificity for CAFs. i) Intersections of DEGs across single-cell and bulk RNA-seq modalities in CAFs. DEGs in the scRNA-seq dataset were determined by grouping all CAF clusters as one, prior to contrasting by genotype. j) Genotyping of cultured CAFs and immortalized dermal fibroblasts (iDFs) compared to somatic DNA. YUMMER1.7 cells [169] are used as a reference for Braf allele recombination. k) Flow cytometric detection of PDGFRa on cultured CAFs. YUMMER1.7 is used as a negative control. l) Western blot showing deletion of macroH2A and accumulation of FOSL2 in dKO cultured CAFs. Histone H4 and NF-κB p65 are used as loading controls for histones and TFs, respectively. m) Expression normalized to housekeeping controls of indicated immediate-early and cytokine genes determined by RT-qPCR in iDFs from WT and dKO mice at the indicated time after serum stimulation.

Supplemental Figure 6. Filipescu et al.

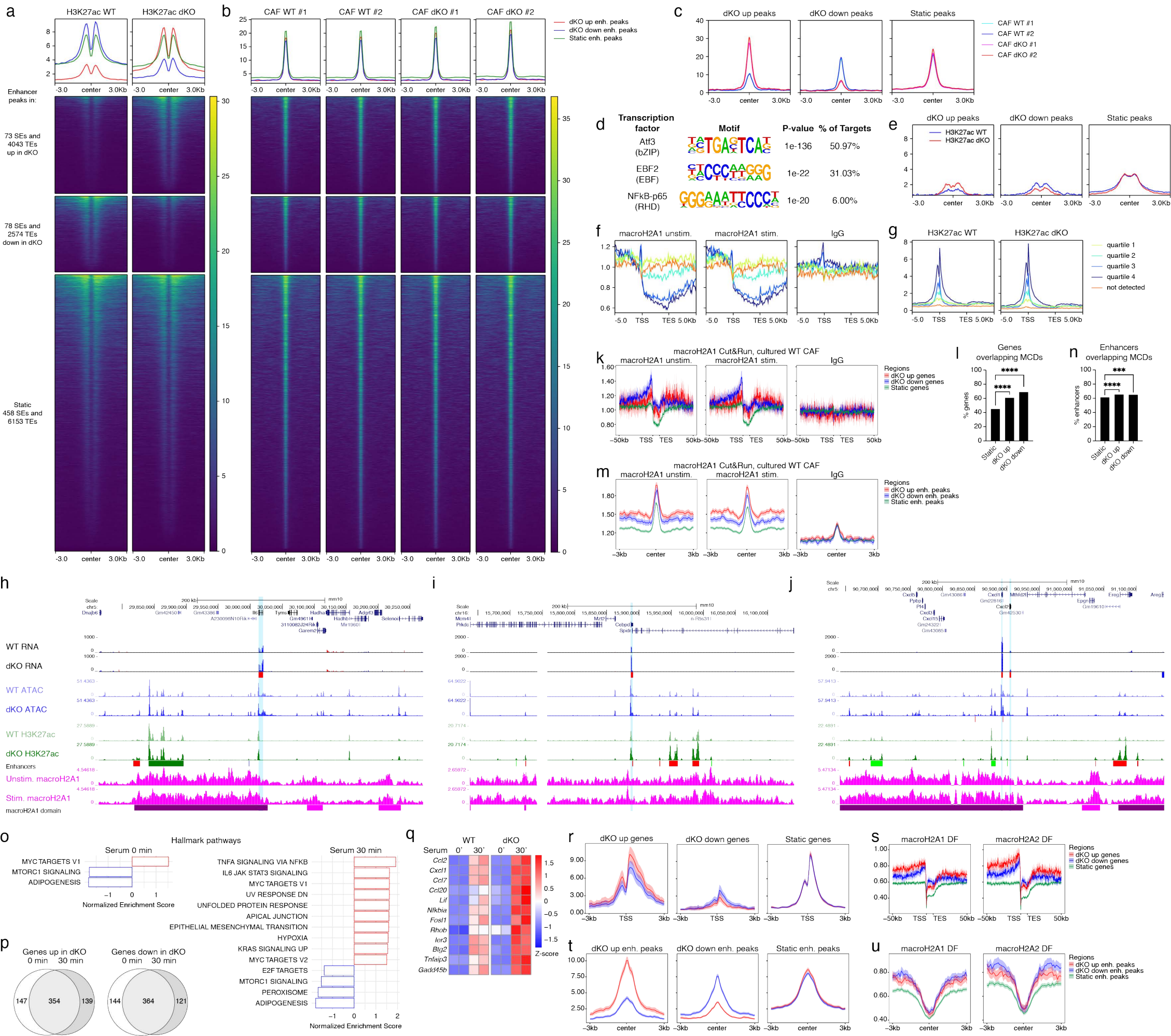

Supplemental Figure 6. Epigenomic analysis in the absence of macroH2A in cultured CAFs and iDFs.

a) Heatmap of H3K27ac ChIP signal in serum-stimulated cultured CAFs centered around ATAC peaks located in enhancers that gain, lose or maintain static H3K27ac levels in dKO vs. WT (n = 6659 in up, 5211 in down, 18961 in static enhancers). Number of TEs and SEs noted for each cluster. b) ATAC-seq signals at peaks in (a). c) Average profile of ATAC-seq signal at differentially accessible regions in dKO vs. WT sorted CAFs. d) Top 3 hits of HOMER TF motif analysis of regions of increased accessibility in dKO vs. WT sorted CAFs. e) H3K27ac ChIP signal in serum-stimulated cultured CAFs at ATAC-seq regions defined in (c). The same scale was used as in A for comaprison. f) Metagene profile of macroH2A CUT&RUN signal in cultured WT CAFs before and after serum stimulation binned into quartiles according to their expression levels. Genes not detected are either not expressed or not mappable. g) Metagene profile of H3K27ac levels in serum-stimulated cultured CAFs as in (f). h-j) UCSC browser screenshots centered around the *Il6, Cebpd, and Cxcl1* loci repectively, 200 kb up- and downstream, of indicated transcriptomic and epigenomic features. Bars under RNA-seq and ATAC-seq tracks indicate significantly up- (red) or downregulated (blue) genes or accessible regions in dKO vs. WT sorted CAFs. Below H3K27ac tracks, bright and dark bars indicate TEs and SEs, respectively; red, blue and green denote gain, loss and no change respectively of H3K27ac level in dKO vs. WT CAFs. Bars under macroH2A1 CUT&RUN tracks indicate domains of macroH2A enrichment, with dark magenta identifying domains concentrating the highest levels of macroH2A1 signal. k) Metagene profile of macroH2A CUT&RUN signal in cultured WT CAFs before and after serum stimulation at genes differentially up, down or static in dKO vs. WT sorted CAFs. l) Percentage of overlap between DEGs and MCDs. Comparison with static genes was

performed using a Chi-square test. **** P-value <0.0001. m) Average profile of macroH2A CUT&RUN signal in cultured WT CAFs before and after serum stimulation at peaks in (a). Note the signal pattern at the center of the ATAC peak, likely due to a bias of CUT&RUN for accessible chromatin sites. n) As in (l), percentage of overlap between peaks in (a) and MCDs **** P-value <0.0001, *** P-value = 0.001. o) Significant Hallmark pathways in GSEA analysis of dKO vs. WT performed in iDFs prior to (0 min) and post serum stimulation (30 min). p) Venn diagrams representing the extent of overlap between pre- and post- serum stimulation in genes up- and downregulated by macroH2A deficiency in iDFs. q) Heatmap of a subset of inflammatory genes hyper-induced by serum stimulation in the absence of macroH2A. r) Average profile of H3K27ac ChIP signal in serum-stimulated WT vs. dKO iDFs at promoters of all differentially-expressed and static genes of matched expression following serum stimulation. s) Average profile of macroH2A1 and macroH2A2 signal in dermal fibroblasts at genes described in (r). t) As in (r), for enhancer peaks differentially enriched in H3K27ac. u) Average profile of macroH2A1 and macroH2A2 signal in dermal fibroblasts at regions described in (t).